

Article

Ultrasonic Preparation of PN for the Photodegradation of 17 β -Estradiol in Water and Biototoxicity Assessment of 17 β -Estradiol after Degradation

Kun Meng¹, Kefu Zhou^{1,*} and Chang-Tang Chang^{2,*}

¹ Laboratory of Ministry of Education for Coastal and Wetland Ecosystems, College of the Environment and Ecology, Xiamen University, Xiamen 361102, China

² Department of Environmental Engineering, National I-Lan University, Yilan 260007, Taiwan

* Correspondence: zhkefu@xmu.edu.cn (K.Z.); ctchang@niu.edu.tw (C.-T.C.)

Abstract: This study prepares a novel phosphorene (PN) and loads it onto TiO₂ to fabricate PN-TiO₂ and effectively photodegrade the hydrophobic environmental hormone 17 β -estradiol in aqueous solutions. The effect of the PN on degradation efficiency is systematically investigated. It is observed that the doping of TiO₂ with PN significantly enhances its photocatalytic and adsorption properties compared with that in the absence of PN; that is, the addition improves the adsorption capability of the composite. The optimal PN weight content is found to be 0.5%. The performance of the PN-TiO₂ photocatalyst in degrading E2 is around 67.5%. However, its photodegradation efficiency gradually decreases when the PN content is further increased. This optimal PN content directly suggests synergistic interactions affecting the photodegrading efficiency. Compared with other PN-based photocatalysts mentioned in the literature, this PN-based material possesses striking advantages, such as higher energy efficiency, greater removal capacity, and superior cost-effectiveness. Further, the decrease in the biotoxicity of the water after treatment is evident in observing the development of zebrafish embryos. The studies of the catalyst performed on the zebrafish show that it results in a higher mortality rate at 96 h with a superior hatching rate and healthy fish development. In summary, the prepared PN-based materials exhibited promising photocatalytic capabilities for the removal and biotoxicity reduction of 17 β -estradiol in aqueous solutions.

Keywords: PN-oxide hybrid; photocatalysis; 17 β -estradiol removal; zebrafish embryos



Citation: Meng, K.; Zhou, K.; Chang, C.-T. Ultrasonic Preparation of PN for the Photodegradation of 17 β -Estradiol in Water and Biototoxicity Assessment of 17 β -Estradiol after Degradation. *Catalysts* **2023**, *13*, 332. <https://doi.org/10.3390/catal13020332>

Academic Editor: Jorge Bedia

Received: 28 December 2022

Revised: 27 January 2023

Accepted: 28 January 2023

Published: 2 February 2023



Copyright: © 2023 by the authors. Licensee MDPI, Basel, Switzerland. This article is an open access article distributed under the terms and conditions of the Creative Commons Attribution (CC BY) license (<https://creativecommons.org/licenses/by/4.0/>).

1. Introduction

For decades, environmental hormones (EHs) have been used extensively to augment agricultural production for exponentially growing population needs. However, although these hormones provide some benefits, they inevitably pose a serious threat to human and wildlife health. In fact, some studies have suggested that EHs have a negative impact on the reproductive systems, nervous systems, and immune systems of organisms, leading to slow and malformed development, decreased sperm counts, poor sperm motility, and increased cancer risks [1–3].

Regarding environmental hormones, 17 β -estradiol (E2) is a typical steroid estrogen used significantly for the reproduction of aquatic organisms even at extremely low concentrations. Biegel et al. [4] reported that this estrogen caused the stripes of male crocodiles to be transformed to that of female crocodiles as well as causing the crocodiles to exhibit female-like reproductive behavior. Diamante [5] also observed that zebrafish embryo underwent some changes, including curved body axis, yolk-sac edema, and pericardial edema, after treatment with E2. Angus [6] reported that high dosages of E2 led to the death of juvenile fishes in water bodies. Consequently, considerable attention has been paid to the development of techniques for the removal of E2, e.g., biodegradation [7–9], ion exchange [10,11], adsorption [12,13], and photocatalysis [14,15].

Although biodegradation could facilitate the decomposition of E2 into inorganic matter to some extent, the applications of biodegradation are still limited due to the long period of degradation and the strict conditions for bacterial growth. Bimetal-organic framework-derived nanotubes and cellulose aerogels have also been studied as photocatalysts for peroxymonosulfate activation [16]. By contrast, ion exchange and adsorption technologies are incapable of degrading E2.

Compared with these methods, photocatalysis is popularly regarded as the most appropriate method for E2 removal due to its high removal efficiency, shorter degradation period, and decomposable intermediates. In the photoreaction process, light irradiates the semiconductor to cause the excitation of electrons from the valence band (VB) to the conduction band (CB), creating positively charged holes (h^+) and negatively charged electrons (e^-) available for photochemistry. This process also accelerates the photocatalysis process, where a catalyst promotes secondary photoreactions due to the formation of the strong oxidizing capabilities of holes and the reduction potentials of electrons [16].

Among typical catalysts (e.g., TiO_2 , CeO_2 , ZnO , SnO_2), TiO_2 is widely used in the photocatalysis process as it is a chemically stable, low-cost, and nontoxic material with promising reusability [17]. Recently, significant attention has been paid to the heterogeneous doping of TiO_2 to enhance adsorption under visible light irradiation by decreasing its band gap and preventing the recombination of electrons and holes. However, several investigations have utilized expensive heavy metals (e.g., Au, Ag, and Pt) as a dopant [18,19], increasing the overall cost and pollution risk. Consequently, an environmentally friendly and biocompatible substitute [20], PN- TiO_2 , has been proposed for the photo-decomposition of E2.

Regarding novel materials, phosphorene (PN) is a novel two-dimensional (2D) material with a high current on/off ratio ($\sim 10^4$ – 10^5) and high electron mobility (~ 200 – $1000\text{ cm}^2\text{V}^{-1}\text{s}^{-1}$) at room temperature. [20,21]. Thus, it can be used to dope TiO_2 , to enhance the excitation of electrons from VB to CB, and inhibit electron-hole recombination, leading to the increased generation of hydroxyl radicals ($\cdot\text{OH}$). Furthermore, Wang et al. [22] reported that $\cdot\text{OH}$ and $^1\text{O}_2$ can be generated when PN is irradiated with ultraviolet (UV) and visible light, respectively. This strongly supports the notion of PN as an electrochemically feasible photocatalyst. Thus, the photocatalytic performance of TiO_2 may be improved if it is doped with PN. In addition, PN possesses a large specific surface area [23] that aids the adsorption of contaminants onto reactive sites at the surface of TiO_2 , significantly promoting the removal of E2.

Previous studies have attempted to employ TiO_2 for the photodegradation of E2. It was found that degradation efficiency increased with increasing TiO_2 concentration. The highest degradation efficiency could be achieved as the TiO_2 concentration rose to 0.5 mg ml^{-1} . However, the degradation efficiency would decrease as the TiO_2 concentration ranged from 0.5 to 1 mg ml^{-1} [24]. Another study achieved 20% removal of E2 at just 60 min of contact time using a TiO_2 photocatalyst compared to a ZnO photocatalyst [24]. Very few studies have been conducted to explore the capabilities of a TiO_2 photocatalyst for E2 degradation, hence the need for further studies.

In this study, PN is fabricated to mix with various amounts (0.5% weight, 1.0% weight, and 3.0% weight) of PN and TiO_2 using microwave heating to synthesize PN- TiO_2 composites (e.g., 0.5% PN- TiO_2 , 1.0% PN- TiO_2 and 3.0% PN- TiO_2). The degradation efficiencies of these composites are investigated to quantify the performance of E2 elimination. Although several studies [14,15,24–26] have investigated the degradation efficiency of TiO_2 or TiO_2 -based composites, the removal capacities reported in these studies were still low and operation inevitably required strong illumination. In this study, only an 8 W UV light source is used to demonstrate the treatability of effective photocatalysis with cost and energy-effectiveness. This study exhibits the most representative PN-based hybrid for the elimination of hydrophobic and refractory pollutants in aqueous solutions [27–31].

2. Results

2.1. Material Characterization

To confirm the formation of composites through sample characterization, TEM, XRD, Raman, FT-IR, XPS, and EDX analyses were performed. The surface morphology of the crystalline composites could be easily observed from TEM images as indicated in Figure 1. Figure 1a clearly exhibits the ultrathin film structure of the samples confirmed to be the characterization of 2D material as it was revealed. Moreover, the electron diffraction patterns of the selected area as shown in Figure 1b also confirmed the crystalline nature of the sample. To further determine the thickness of the PN, the AFM characterization technique was applied through an optical contrast analysis (Figure 2a). The results indicated that the clear edges of the PN were still sharpened, suggesting that oxidation was unlikely to have occurred during material preparation. Moreover, the height profile from Figure 2b showed that the thickness of the PN was approximately 3.0–5.0 nm. According to Liu et al. [2], the thickness of a single layer of PN is approximately 0.9 nm, suggesting that the number of sample layers could have been approximately 3–5. This is consistent with the findings of the TEM.

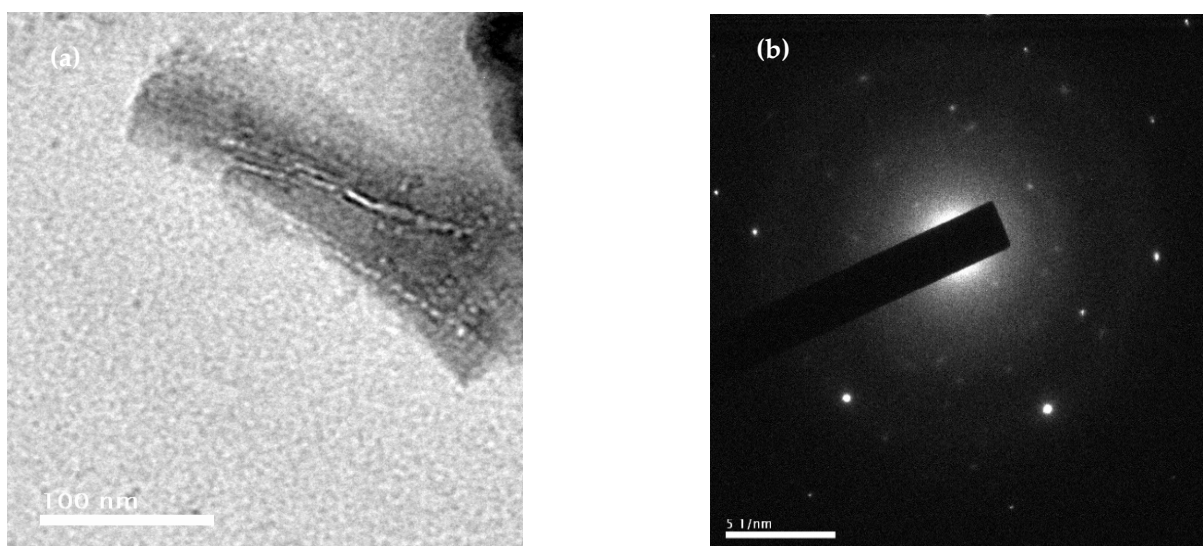


Figure 1. (a) TEM image and (b) electron diffraction pattern of PN.

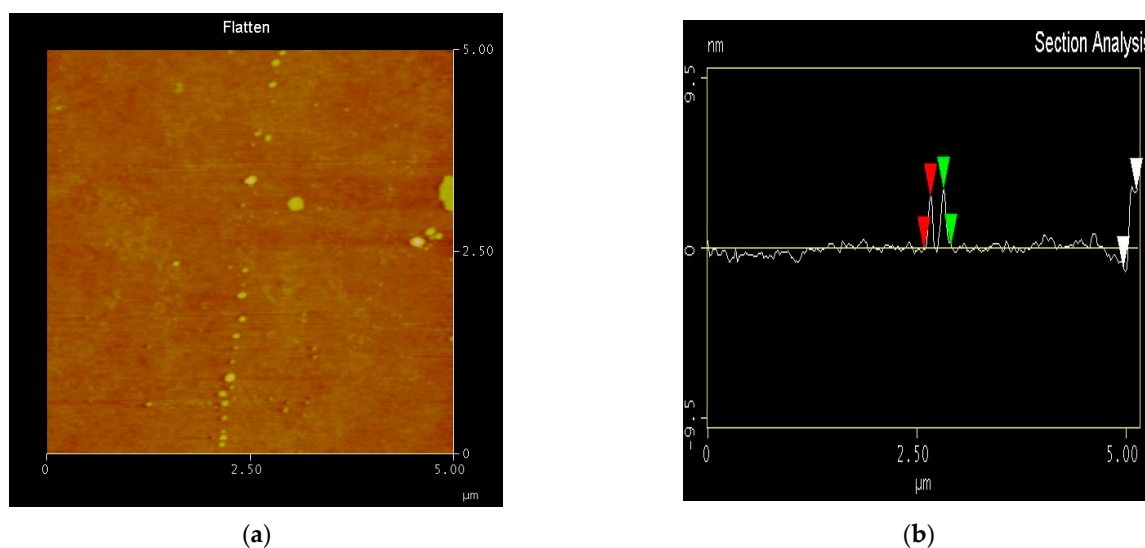


Figure 2. AFM spectra of composite (a) external surface morphology (b) height profile.

To identify the substructure and electronic features of PN and PN-TiO₂ composite, Raman spectra were implemented as shown in Figure 3. The results indicated that three Raman characteristic peaks of black phosphorous (BP) and PN were displayed at approximately 361 cm⁻¹, 436 cm⁻¹ and 463 cm⁻¹. These peak wavelengths corresponded to phosphorous. It was confirmed that the second sample prepared was indeed a phosphorous homologous substance. An apparent shift was observed for the composite samples at 361 cm⁻¹ and 463 cm⁻¹, indicating a comparatively smaller thickness than that of BP. This was due to a positive relationship between the extent of the shift and the PN thickness as reported in the literature [1]. There were more and less obvious additional peaks at 144 cm⁻¹ and 391 cm⁻¹, respectively, in the Raman spectroscopy of PN-TiO₂. The two characteristic peaks corresponded to the typical figure of Raman spectra for anatase, directly indicating that the TiO₂ sample was P25 and the ratio of anatase to rutile was 80/20 [2]. Moreover, the formation of three signals identified the approximate locations of 361 cm⁻¹, 436 cm⁻¹ and 463 cm⁻¹ in the curve of PN-TiO₂ composites, suggesting that PN was successfully combined with TiO₂ [3].

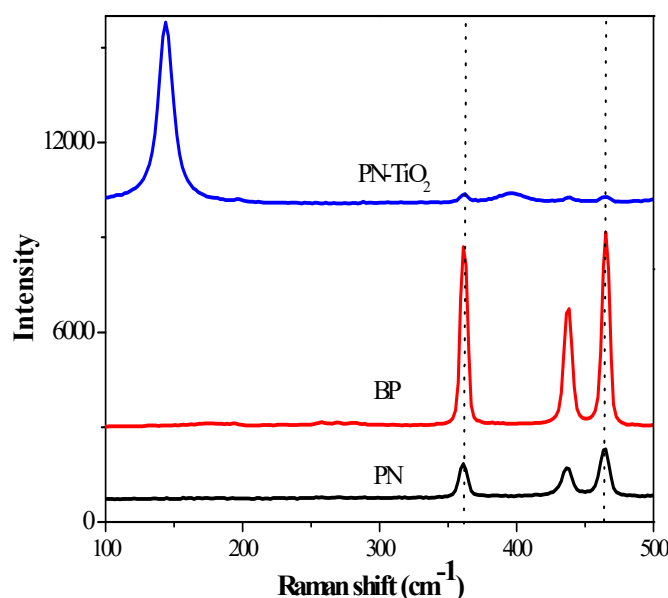


Figure 3. Raman spectra of BP, PN, and PN-TiO₂.

In addition, XRD patterns of the samples were obtained to reveal the crystalline structure and phase purity of TiO₂ (Figure 4). Figure 4 illustrates the apparent peaks for (*hkl*) 020 and 040 planes according to JCPDS card no. 47-1626. The results of both the TEM and AFM confirmed that the PN was prepared successfully. All the relatively high characteristic peaks in the XRD image of the TiO₂ reflected its anatase structure. The TiO₂ used in this study was P25 with anatase at approximately 80%. The absence of the characteristic peaks of other impurities simply suggests the high purity of the composites studied.

To observe the changes in the absorption spectra of these four composites with different PN content levels at 0.5% PN-TiO₂, 1.0% PN-TiO₂, and 3.0% PN-TiO₂, a UV-vis spectrophotometric analysis was carried out at a range between 200 nm and 800 nm (Figure 5). As indicated in Figure 5, its results directly pointed out that gradually increasing capacities of adsorption within visible light ranges occurred with the increase in PN content. Although there was a slight decrease in the adsorption value within UV light, the E_g value of these composites determined by Equation (1) was still lower, and the order of this decrease in adsorption was as follows: E_g3.0% PN-TiO₂ (2.6 eV) < E_g1.0% PN-TiO₂ (2.8 eV) ≈ E_g0.5% PN-TiO₂ (2.8 eV) < E_gTiO₂ (3.0 eV)

$$E_g = 1240/\lambda \quad (1)$$

where parameter λ is the node value of the tangent of the spectra and X axis.

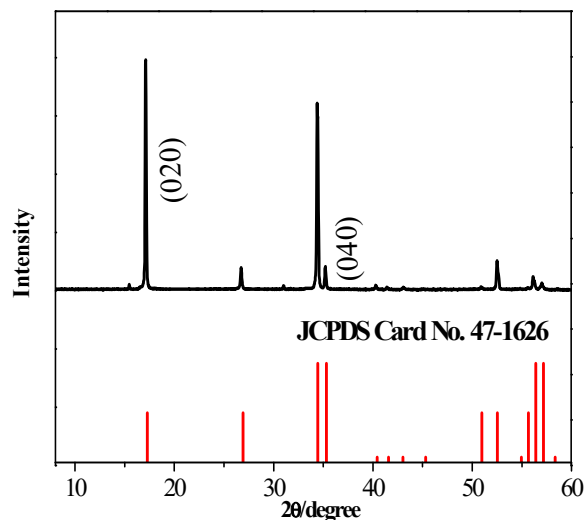


Figure 4. XRD pattern of TiO₂.

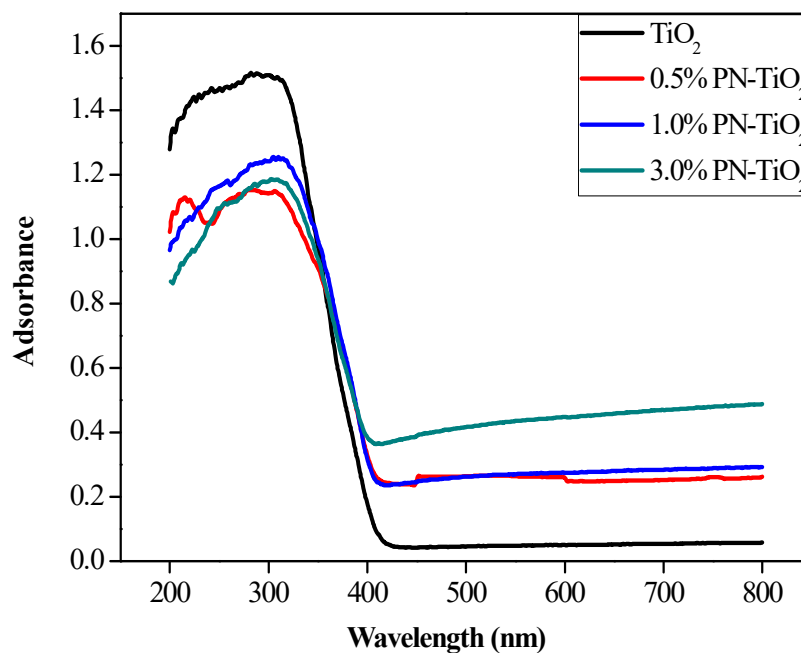


Figure 5. UV-vis absorption spectra of PN-TiO₂ with various PN content levels.

To explore the characterization of material preparation, the surface morphology of PN-TiO₂ was also studied via SEM (Figure 6a). As the SEM image indicated, the particle of TiO₂ was evenly distributed with nearly no particle aggregation. Figure 6b shows a typical EDS image of the PN-TiO₂ composite. The EDS image showed that the composite consisted of P, Ti, and O elements. Combining the results obtained from both Figure 6c and the elemental maps of PN-TiO₂, the three elements were completely mixed and P was successfully loaded onto TiO₂.

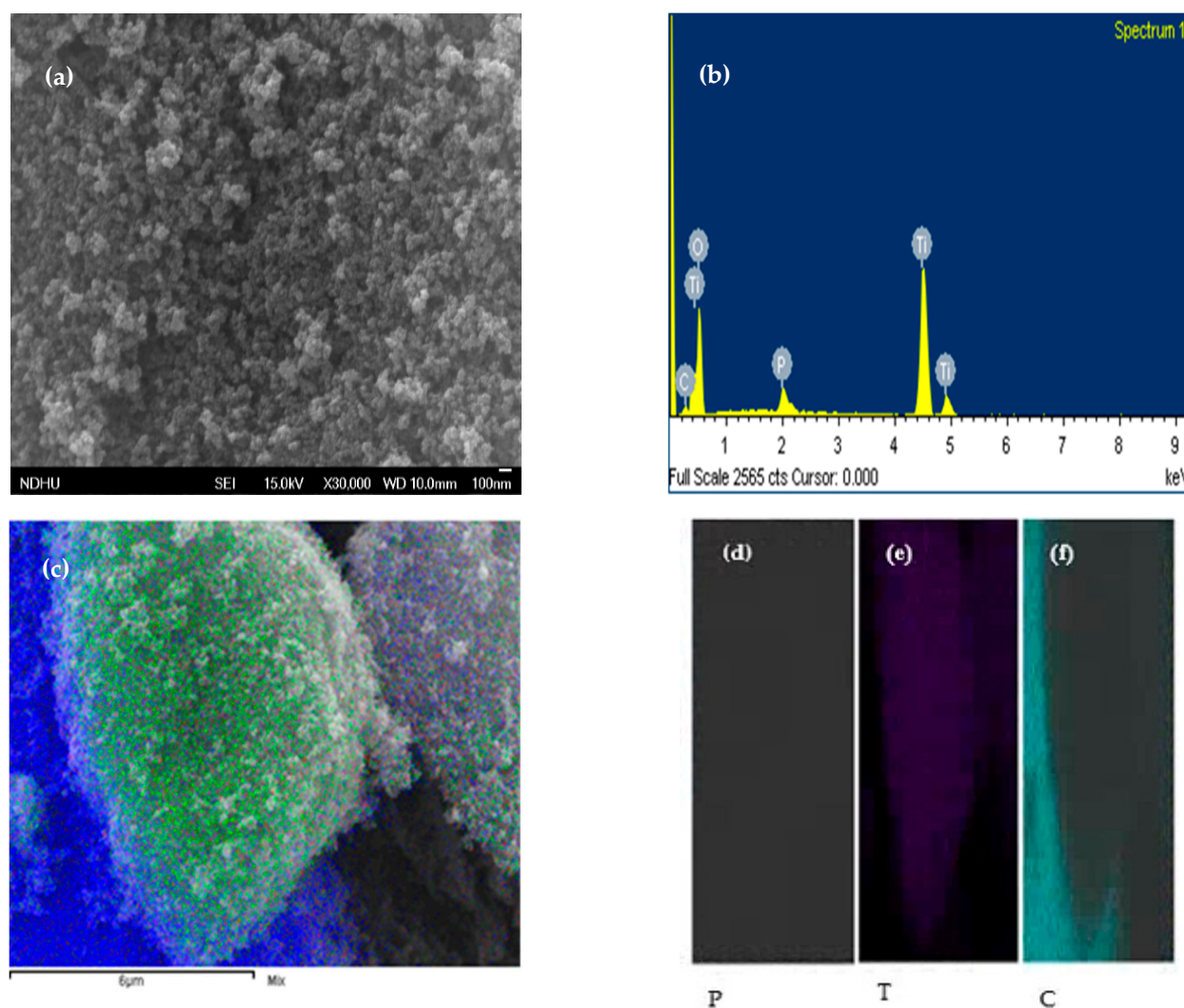


Figure 6. SEM images: (a) SEM spectrum, (b) EDS of PN-TiO₂ composite, (c) overlapping of P, Ti, and C elements, (d–f) elemental maps of 3% PN-TiO₂.

2.2. Photodegradation Performance of PN-TiO₂

2.2.1. Effects of Different Levels of PN Content

To investigate the photocatalytic efficiency of composites with different levels of PN content, 0.05 g of TiO₂, 0.50% PN-TiO₂, 1% PN-TiO₂, and 3.00% PN-TiO₂ were individually mixed with 500 mL of 10 ppm E2 solution for comparative study (Figure 7). As Figure 7 indicates, the removal of E2 was significantly improved with an increase in PN content. In addition, bare TiO₂ was observed to be more hydrophilic, leading to the lower adsorption of E2 on the surface of the catalyst. However, it is observed that the photodegradation of E2 was enhanced for 0.5% PN, but a further increase in the PN content decreased degradation performance. This may be attributed to the fact that PN as an electron acceptor may prevent electron-hole recombination caused by TiO₂ [31–35]. Moreover, h⁺ may react with water and oxygen to generate ·OH to eliminate E2, as shown in Equations (2)–(6). ·OH can also be generated due to the excitation of PN by UV light [22]. Thus, increased photodegradation efficiency is shown where PN is doped into TiO₂. However, the excessive PN content still affected the absorption of the catalyst, leading to decreased catalytic activity. This was confirmed by the UV–vis absorption spectra of PN-TiO₂ (Figure 5). Furthermore, it was also observed that PN could be significantly accumulated when PN content was very high;

thus, it could not prevent electron-hole recombination. Consequently, the catalytic activity of the PN-TiO₂ composite was attenuated [35].

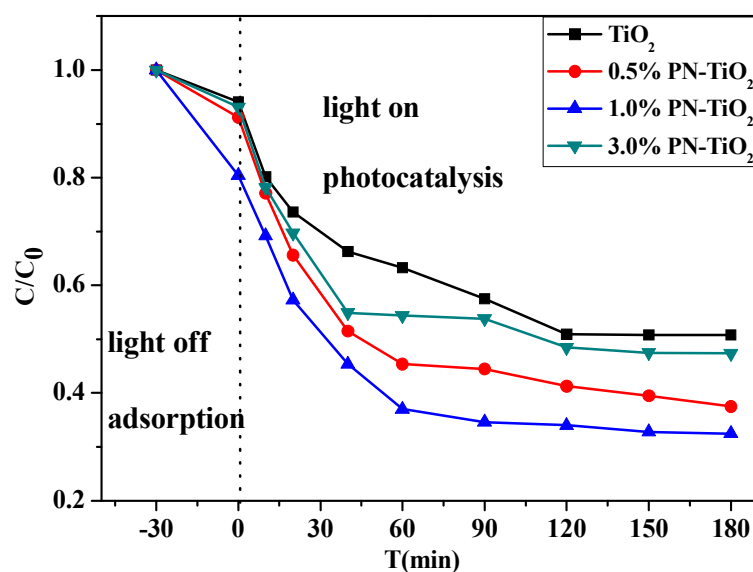
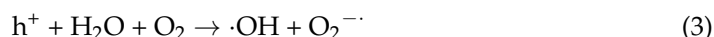


Figure 7. Photodegradation efficiency of different PN-TiO₂ composites. ($t < 0$ and $t > 0$ denoted dark adsorption and light photocatalysis, respectively).

2.2.2. The Biototoxicity of the Water after Degradation

To evaluate the biotoxicity of the treated water, zebrafish were used as the model organism. Ten fish in each group were exposed to the clean water (group 1), the wastewater containing E2 (group 2), and the treated water (group 3), respectively [36]. The hatching rates, mortality rates, and heart rates were observed to investigate the effects of the water before and after degradation on the development of zebrafish embryos. Thus, it could be determined whether the photocatalysis degradation system was effective.

Figure 8 shows that heart rates increased with the development of the embryos in a natural environment (group 1), which was in contrast to those in the water containing E2 (group 2 and group 3). Heart rates in group 3 were slightly higher in the beginning and then decreased with time accumulation. This indicates that a certain concentration of E2 may lead to some response within a short timeframe; however, a biotoxicity effect emerged afterward, causing heart rates in group 3 to decrease at 48–96 h. Furthermore, a significant decrease was observed in group 2, demonstrating that higher concentrations of E2 have a negative effect on the metabolic activity of zebrafish embryos and inhibit their growth. These results correspond with those of Ulhaq [37]. In addition, the difference between group 2 and group 3 shows that photocatalysis degradation decreased the activity of E2 and its biotoxicity.

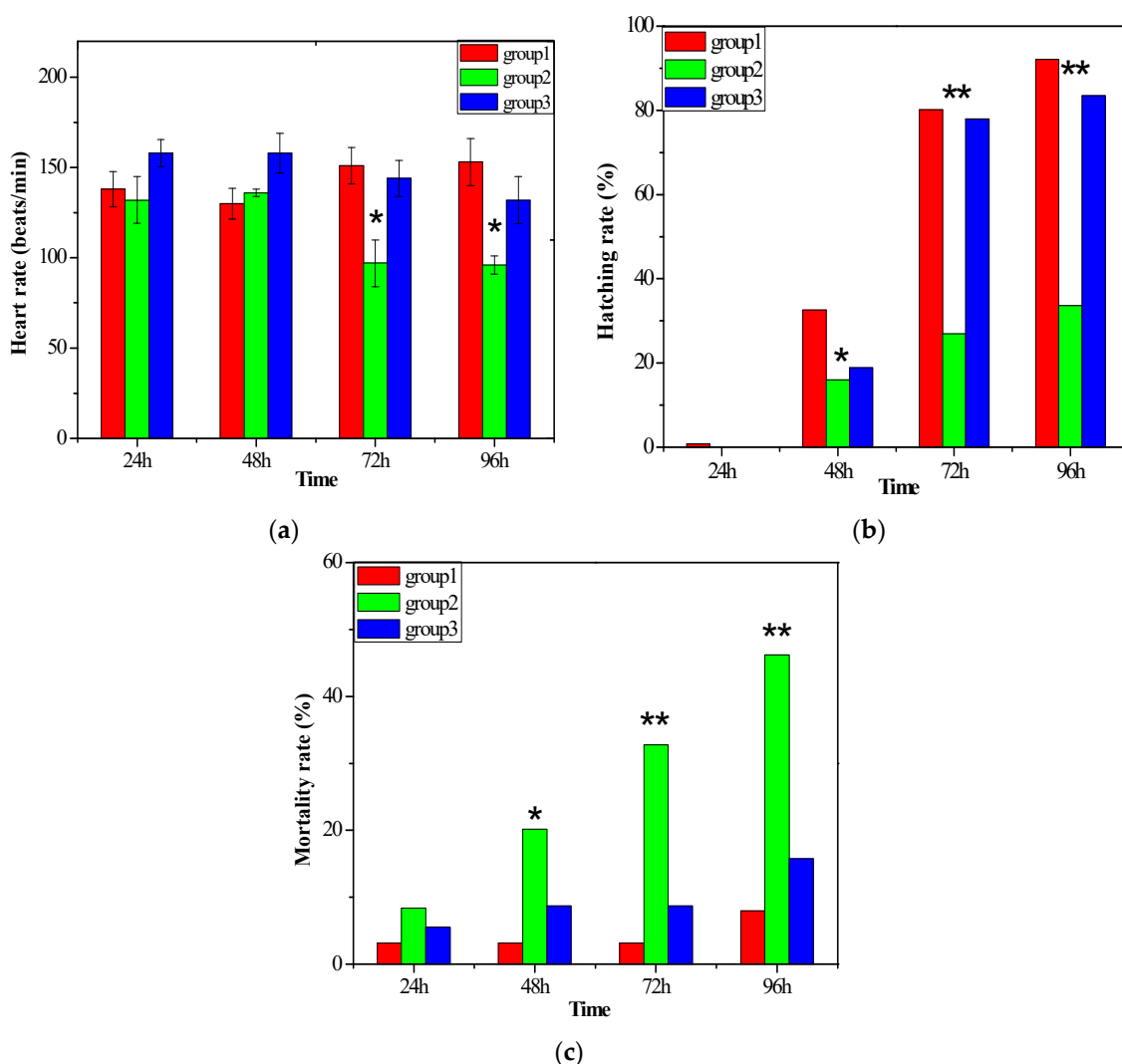


Figure 8. The heart rates (a), hatching rates (b), and mortality rates (c) of zebrafish embryos in three groups (* in each graph indicated significant differences, $p < 0.05$; ** in each graph indicated very significant differences, $p < 0.005$).

According to Figure 2, zebrafish eggs started to hatch out from the second day, and the highest hatching rate appeared on the third day. However, there was a significant difference between the hatching rate of group 2 and those of the other two groups. Furthermore, the hatching rate in group 2 was significantly lower throughout the whole hatching process, which demonstrates that a higher concentration of E2 inhibits the development of zebrafish embryos leading to lower hatching rates, which is consistent with the findings of a report by Lee [38]. There was also no significant difference between group 1 and group 3, indicating that the water environment in the two groups was similar.

Figure 3 shows that the mortality rate of embryos became higher in the 3 groups with the accumulation of time, and the mortality rate was highest in group 2. It can be inferred that higher E2 concentrations may lead to the higher mortality of zebrafish embryos. A study by Ren [39] also mentioned that higher levels of E2 ($>10 \mu\text{M}$) would lead to zebrafish malformation or mortality. Moreover, it can be observed that the mortality rate of zebrafish embryos in group 3 was significantly lower than that in group 2 and was similar to that in group 1, suggesting that the water degradation led to the lower mortality rate of zebrafish embryos.

In conclusion, the photocatalysis system was effective for the degradation of E2 and could decrease the negative effects of E2 on the development of zebrafish embryos.

3. Discussion

3.1. Comparative Assessment of Degradation Performance

To compare the degradation efficiencies of other materials, the degradation performances of similar materials obtained from the literature were adopted (Table 1). Evidently, the results of this study indicated that the removal rate and photocatalytic capacity of the model used in our study are promising. Its efficiency with the 10 ppm E2 solution led to an achievement of 79.5% removal within 3 h, which was a far superior result to those in reported data [14,15,24,25]. For example, its removal capacity was 39.8 mg/g. Alvarez-Corena [36,37] reported that degradation efficiency was significantly enhanced when O₂ was added to pure TiO₂ for E2-containing wastewater treatment. In addition, the degradation rate was 0.53 min⁻¹, which is 5–10 times higher than that reported in other studies. However, O₂ was required to be supplied continuously during this process, inevitably leading to a higher cost for practical applications. Li et al. [38] and Fernandez [39] reported degradation efficiencies of 99.5% and 90% when Fe-Bi₂SiO₅ and P25 were utilized to decompose E2 at 3 ppm and 1 ppm in an aqueous solution, respectively. According to the Langmuir–Hinshelwood mechanism, these higher efficiencies were likely attributed to the lower E2 concentration. Consequently, their removal capacities were approximately 5.97 mg/g and 1.80 mg/g, which were around 1/8 and 1/20 times lower than that in our study, respectively. Moreover, a high-intensity UV lamp was still required to be used in these two studies and cost-effectiveness problems were still of great concern. Yang et al. [26] used a 20 W UV lamp in their study. FTG (surface fluorinated TiO₂/reduced graphene oxide) and TiO₂-RGO (reduced graphene oxide) were prepared to remove 3 ppm of E2 solution, and their degradation efficiencies reached up to 99.8% and 83.3% in 180 min, respectively. These efficiencies were higher than that of P25 (74.4%) and of the model in our study (79.5%). FTG in particular was capable of completely removing 3 ppm of E2 in wastewater in 3 h. This is possibly due to the vital role of F⁻ in photocatalysis. The adsorption of F⁻ on the surface of TiO₂ improved the crystallization of the TiO₂ anatase phase. However, the ·OH radicals generated on the surface of F-TiO₂ were more mobile than those generated on pure TiO₂ under UV irradiation [40]. Further, F⁻ is harmful to the environment and ecosystem, meaning that a secondary pollutant could be generated without recycling. Furthermore, a UV lamp of a higher intensity was used in the study, and the removal capacity was still far lower than our study.

Table 1. Comparison of degradation efficiency and removal capacity of this study with the literature.

Reference	Materials	C ₀ (L ⁻¹) *	Degradation Efficiency	Light Source	K ₁ * (min ⁻¹)	Removal Capacity * (mg/g)
[24]	Immobilized TiO ₂	44 µg	45% (180 min)	36 W UV	0.003	0.0132
[37]	TiO ₂ + O ₂	2 mg	93% (25 min)	100 W UV	0.53	18.6
[15]	TiO ₂ -FeZ	1.36 mg	78.1% (90 min)	450 W Xe lamp	0.015	25.3
[26]	FTG4	3 mg	99.8% (180 min)	20 W UV	0.035	Unsaturation
[26]	TiO ₂ -RGO	3 mg	83.3% (180 min)	20 W UV	0.010	8.33
[26]	P25	3 mg	74.4% (180 min)	20 W UV	0.008	7.44
[14]	NTT	0.54 mg	65% (150 min)	3300 µW/cm ² UV	0.007	3.51
[38]	Fe-Bi ₂ SiO ₅	3 mg	99.5% (60 min)	20 W UV	0.069	5.97
[39]	P25	1 mg	90% (3 h)	64 W UV	0.013	1.8
[25]	4%GO-TiO ₂	1 mg	48% (60 min)	450 W Xe lamp	0.011	24
This study	PN-TiO ₂	10 mg	79.5%	Visible/UV	0.006	67.5

* C₀ is the initial concentration; K₁ is the first order constant; removal capacity = mass of pollutant (mg)/mass of material (g).

This study used a PN and PN-TiO₂ composite as a photocatalyst. Although the mass% of the PN was only 0.5% in the composite, its degradation efficiency was more significantly improved than that of bare TiO₂. Furthermore, our use of a UV lamp with very low intensity (8 W) suggests that this technique is not only cost-effective but also energy-efficient. This is consistent with the aim of green sustainability and environmental friendliness. The removal capacity of 39.8 mg/g was still far higher than that reported in the literature (Table 2). However, the degradation rate still requires further improvement from a kinetic perspective for overall performance consideration.

Table 2. PN and PN-based hybrids and their fields of application.

Reference	Material	Field of Application
[27]	PN–GN hybrid	Perpendicular electric field
[28]	PN–GN hybrid	Schottky barrier diode
[29]	PN–MoS ₂	Electric field/solar cell
[30]	PN–h–BN	Electric field
[22]	PN	Photocatalysis for DPBF
[31]	(more)PN–TiO ₂	Photocatalysis for dye
This study	(less)PN–TiO ₂	Photocatalysis for 17β-estradiol

PN, GN, BN, and DPBF indicate phosphorene, graphene, hexagonal boron nitride, and 1,3-diphenylisobenzofuran, respectively.

3.2. Significance of this Study

Recently, a novel 2D material, PN, has attracted considerable attention in studies owing to its physical, electrical, and chemical characteristics. Most of these studies have focused on the electrical applications of PN (e.g., solar cells and barrier diodes) [27–30], and a few studies have investigated its photocatalytic properties (Table 2). In addition, degradation efficiency [33] and catalyst instability were mentioned when PN was used as a photocatalyst, as it could readily react with water and oxygen to generate PO₄^{3−} [31,41,42]. In this study, PN was mixed with the commonly used oxide TiO₂ to prepare a PN–TiO₂ hybrid. The advantages of this hybrid can be summarized as follows: (1) PN exhibited synergistic interactions with photodegradation due to its inherent photocatalytic properties; (2) The proposed doping of PN (instead of expensive metals) into TiO₂ was biocompatible and cost-effective; and (3) PN–TiO₂ composites were stable, preventing the reaction of PN with water and oxygen. Lee et al. [31] reported black phosphorus (BP) @TiO₂ as a promising photocatalyst for dye photodegradation. However, the mass content of PN was very high in this composite, thus increasing the overall cost, since PN is still not economically feasible compared with TiO₂ [42,43]. Regarding synergistic photocatalysis, PN inhibits electron-hole recombination due to its high electron mobility, improving the degradation efficiency of the hybrid for pollutant elimination. Moreover, the addition of PN increased degradation efficiency by 30% in the aqueous phase compared to that exhibited by bare TiO₂. The maximum degradation efficiency was achieved at an optimum PN content at 1.0% wt. Thus, the overall cost was still far lower than that of the model reported by Lee [38]. This study indicates the considerable prospects of the fabrication of other PN–oxide hybrids (e.g., PN–WO₃ and PN–CeO₂) that may exhibit comparable photodegradation performance.

4. Material and Methods

4.1. Chemical Reagents

Bulk black phosphorus (BP) was obtained from XFNANO. Model pollutant 17β-estradiol (E₂, purity ≥ 98%) was purchased from Sigma. Nano-TiO₂ was provided by ACROS. Ultrapure hydroelectricity was prepared using the OTUN ultrapure water system (0R007XXM1, ELGA). Stock solutions of E₂ were prepared by dissolving approximately 0.1 mg of E₂ in 100 mL of methanol and stirring well for 5 min. The solution was then maintained at 4 °C for further use.

4.2. Preparation of Phosphorene Nanosheets (PN) and Phosphorene–TiO₂ Composites (PN–TiO₂)

PN was prepared by exfoliating the bulk black phosphorous in liquid via ultrasonic treatment. Sequentially, 25 mg of bulk sample was dispersed into 50 mL ethanol (purity ≥ 99.5%) followed by purging N₂ to remove residual dissolved oxygen (i.e., crucial step preventing PN oxidation). Then, the mixture was placed in ice water for 12 h sonication. The brown suspension was centrifuged at 3000 rpm for 10 min to harvest the supernatant. Then, the solution was bubbled with N₂ for 5 min and then maintained in 4 °C for preparation of PN–TiO₂. The supernatant was then dried at 60 °C for approximately 8 h to obtain PN powder. Hereafter, PN content at 0.5%, 1.0%, and 3.0% was used to mix with TiO₂, which was then added to 15 mL DI water. Next, the solutions were well stirred under

ultrasonication for 1 h and then microwaved (200 °C, 400 W) for 30 min. Finally, the mixtures were dried at 60 °C to harvest PN-TiO₂ composites (denoted as 0.5% PN-TiO₂, 1.0% PN-TiO₂, and 3.0% PN-TiO₂, respectively). The characterizations of PN and PN-TiO₂ were then implemented via transmission electron microscope (TEM, JEM-F200 "F2", Taipei, Taiwan), atomic force microscope (AFM, NX7 ST Instruments, Taipei, Taiwan), Raman spectroscopy (DXR3 SmartRaman Spectrometer, Taipei, Taiwan), X-ray diffraction (XRD, Bruker D2 phaser, Yilan, Taiwan), UV–vis spectrophotometer (Hitachi U-3900, Yilan, Taiwan), field emission scanning electron microscope (FE-SEM, Jeol IT-100, Yilan, Taiwan), energy dispersive spectrometer (EDS, Jeol IT-100, Yilan, Taiwan), and elemental maps.

4.3. Photodegradation Reaction

The cylindrical reactor (7 cm diameter and 40 cm height) was used for the treatability study of photocatalytic degradation. In addition, an 8 W UV lamp (0.55 mW/cm²) and a tungsten halogen lamp (500 W output power) as sources of minimum energy supply were equipped to provide sufficient energy to trigger photodegradation process to take place. Subsequently, 0.05 g of PN-TiO₂ was supplemented into 500 mL of 10 ppm E₂ diluted in 2% methanol diluted with DI water. The reaction was first conducted in the dark for 30 min to achieve equilibrium for absorption, and then UV light was switched on to trigger photocatalysis. All the experiments were conducted at inherent solution pH and 30 ± 0.2 °C at 300 rpm. The samples were then conducted (without removing photocatalysts) using a Millipore filter with pore size of 0.22 µm. E₂ concentration of samples was analyzed through high-performance liquid chromatography (HPLC, ThermoFisher, Yilan, Taiwan). The flow phase was a solution mixture of ultrapure water and acetonitrile in 48:52 volumetric ratio eluting the pollutant with 1.2 mL/mins of flow rate. In addition to 20 µL of injection volume and 25 °C of column, the retention time was set to 5.5 min for E₂.

5. Conclusions

The enhanced photodegradation of 17β-estradiol by phosphorene-basing composites was reported with the successful preparation of PN and PN-TiO₂ photocatalysts through detailed characterization. The extent of the degradation of E₂ reached up to 67.5% with PN-TiO₂ under UV light within 180 min, which was an almost two-fold greater result than that of bare TiO₂. To the best of our knowledge, this study represents the first attempt to combine PN with other catalysts for the degradation of refractory and hydrophobic pollutants (e.g., E₂). During the reaction process, PN could adsorb E₂ onto the surface of TiO₂. The studies of the catalyst performed on zebrafish showed a higher mortality rate at 96 h as well as a superior hatching rate and healthier fish development. Thus, it could facilitate photodegradation due to the formation of the ·OH radical. In addition, the combination of e⁻ with h⁺ could be restrained by PN and could also generate ·OH in combination with TiO₂ to attack E₂, which is the reason why the E₂ degradation efficiency and removal capacity of PN-TiO₂ were higher than that of bare TiO₂. However, some intermediates with high estrogen activity could possibly be produced during this photodegradation process, causing a potential threat to aquatic organisms and humans [5].

Author Contributions: Conceptualization, K.M. and C.-T.C.; methodology, K.Z., K.M.; investigation, K.M. and C.-T.C.; data curation, C.-T.C.; writing—original draft preparation, C.-T.C.; writing—review and editing, C.-T.C.; supervision, K.Z.; project administration, K.Z.; funding acquisition, K.Z. All authors have read and agreed to the published version of the manuscript.

Funding: This work was supported by the National Key Research and Development Program of China (2016YFC0502901) and the National Key Research and Development Program of China (2017YFC0506103). The authors would like to thank the ministry of Science and Technology of Taiwan for providing financial support for project MOST 106-2622-E-197-003-CC3.

Data Availability Statement: Not available.

Conflicts of Interest: The authors declare no conflict of interest.

References

1. Finn, R.S.; Aleshin, A.; Slamon, D.J. Targeting the cyclin-dependent kinases (CDK) 4/6 in estrogen receptor-positive breast cancers. *Breast Cancer Res.* **2016**, *18*, 17. [[CrossRef](#)] [[PubMed](#)]
2. Pendse, S.; Maertens, A.; Rosenberg, M.; Roy, D.; Fasani, R.; Vantangoli, M.; Madnick, S.; Boekelheide, K.; Fornace, A.; Odwin, S.-A. Information-dependent enrichment analysis reveals time-dependent transcriptional regulation of the estrogen pathway of toxicity. *Arch. Toxicol.* **2017**, *91*, 1749–1762. [[CrossRef](#)] [[PubMed](#)]
3. Sanders, J.; Coulter, S.; Knudsen, G.; Dunnick, J.; Kissling, G.; Birnbaum, L. Disruption of estrogen homeostasis as a mechanism for uterine toxicity in Wistar Han rats treated with tetrabromobisphenol A. *Toxicol. Appl. Pharmacol.* **2016**, *298*, 31–39. [[CrossRef](#)] [[PubMed](#)]
4. Biegel, L.B.; Hirshfield, A.N.; O'Connor, J.C.; Ladics, G.S.; Cook, J.C.; Frame, S.R.; Flaws, J.A.; Elliott, G.S.; Silbergeld, E.K.; Van Pelt, C.S.; et al. 90-Day Feeding and One-Generation Reproduction Study in Crl:CD BR Rats with 17 β -Estradiol. *Toxicol. Sci.* **1998**, *44*, 116–142. [[CrossRef](#)] [[PubMed](#)]
5. Diamante, G.; Menjivar-Cervantes, N.; Leung, M.S.; Volz, D.C.; Schlenk, D. Contribution of G protein-coupled estrogen receptor 1 (GPER) to 17 β -estradiol-induced developmental toxicity in zebrafish. *Aquat. Toxicol.* **2017**, *186*, 180–187. [[CrossRef](#)] [[PubMed](#)]
6. Angus, R.A.; Stanko, J.; Jenkins, R.L.; Watson, R.D. Effects of 17 α -ethynylestradiol on sexual development of male western mosquitofish (*Gambusia affinis*). *Comp. Biochem. Physiol. Part C Toxicol. Pharmacol.* **2005**, *140*, 330–339. [[CrossRef](#)] [[PubMed](#)]
7. Li, M.; Zhao, X.; Zhang, X.; Wu, D.; Leng, S. Biodegradation of 17 β -estradiol by Bacterial Co-culture Isolated from Manure. *Sci. Rep.* **2018**, *8*, 3787. [[CrossRef](#)]
8. Xiong, W.; Peng, W.; Liang, R. Identification and genome analysis of *Deinococcus actinosclerus* SJTR1, a novel 17 β -estradiol degradation bacterium. *3 Biotech* **2018**, *8*, 433. [[CrossRef](#)]
9. Yu, Q.; Wang, P.; Liu, D.; Gao, R.; Shao, H.; Zhao, H.; Ma, Z.; Wang, D.; Huo, H. Degradation characteristics and metabolic pathway of 17 β -estradiol (E2) by *Rhodococcus* sp. DS201. *Biotechnol. Bioprocess Eng.* **2016**, *21*, 804–813. [[CrossRef](#)]
10. Mazlan, W.S.; Mokhtar, H.; Saâ, N.; Tajuddin, R.M. Fabrication of ultrafiltration membrane using additive to extract hormone from poultry wastewater. *J. Teknol.* **2016**, *78*, 121–126. [[CrossRef](#)]
11. Tong, Y.; McNamara, P.J.; Mayer, B.K. Fate and impacts of triclosan, sulfamethoxazole, and 17 β -estradiol during nutrient recovery via ion ex-change and struvite precipitation. *Environ. Sci. Water Res. Technol.* **2017**, *3*, 1109–1119. [[CrossRef](#)]
12. Jiang, L.-H.; Liu, Y.-G.; Zeng, G.-M.; Xiao, F.-Y.; Hu, X.-J.; Hu, X.; Wang, H.; Li, T.-T.; Zhou, L.; Tan, X.-F. Removal of 17 β -estradiol by few-layered graphene oxide nanosheets from aqueous solutions: External influence and adsorption mechanism. *Chem. Eng. J.* **2016**, *284*, 93–102. [[CrossRef](#)]
13. Jiang, L.; Liu, Y.; Liu, S.; Hu, X.; Zeng, G.; Hu, X.; Liu, S.; Liu, S.; Huang, B.; Li, M. Fabrication of β -cyclodextrin/poly (l-glutamic acid) supported magnetic graphene oxide and its adsorption behavior for 17 β -estradiol. *Chem. Eng. J.* **2017**, *308*, 597–605. [[CrossRef](#)]
14. Kim, S.; Cho, H.; Joo, H.; Her, N.; Han, J.; Yi, K.; Kim, J.-O.; Yoon, J. Evaluation of performance with small and scale-up rotating and flat reactors; photocatalytic degradation of bisphenol A, 17 β -estradiol, and 17 α -ethynyl estradiol under solar irradiation. *J. Hazard. Mater.* **2017**, *336*, 21–32. [[CrossRef](#)]
15. Kovacic, M.; Kopic, N.; Kusic, H.; Bozic, A.L. Solar driven degradation of 17 β -estradiol using composite photocatalytic materials and artificial irradiation source: Influence of process and water matrix parameters. *J. Photochem. Photobiol. A Chem.* **2018**, *361*, 48–61. [[CrossRef](#)]
16. Saravanan, R.; Gracia, F.; Stephen, A. Basic principles, mechanism, and challenges of photocatalysis. In *Nanocomposites for Visible Light-Induced Photocatalysis*; Springer: Berlin/Heidelberg, Germany, 2017; pp. 19–40.
17. Xing, Z.; Zhang, J.; Cui, J.; Yin, J.; Zhao, T.; Kuang, J.; Xiu, Z.; Wan, N.; Zhou, W. Recent advances in floating TiO₂-based photocatalysts for environmental application. *Appl. Catal. B Environ.* **2018**, *225*, 452–467. [[CrossRef](#)]
18. Tahir, K.; Ahmad, A.; Li, B.; Nazir, S.; Khan, A.; Nasir, T.; Khan, Z.; Naz, R.; Raza, M. Visible light photocatalytic inactivation of bacteria and photo degradation of methylene blue with Ag/TiO₂ nanocomposite prepared by a novel method. *J. Photochem. Photobiol. B Biol.* **2016**, *162*, 189–198. [[CrossRef](#)]
19. Vaiano, V.; Iervolino, G.; Sannino, D.; Murcia, J.; Hidalgo, M.; Ciambelli, P.; Navío, J. Photocatalytic removal of patent blue V dye on Au-TiO₂ and Pt-TiO₂ catalysts. *Appl. Catal. B Environ.* **2016**, *188*, 134–146. [[CrossRef](#)]
20. Bagheri, S.; Mansouri, N.; Aghaie, E. Phosphorene: A new competitor for graphene. *Int. J. Hydrog. Energy* **2016**, *41*, 4085–4095. [[CrossRef](#)]
21. Khandelwal, A.; Mani, K.; Karigerasi, M.H.; Lahiri, I. Phosphorene—the two-dimensional black phosphorous: Properties, synthesis and applications. *Mater. Sci. Eng. B* **2017**, *221*, 17–34. [[CrossRef](#)]
22. Wang, H.; Jiang, S.; Shao, W.; Zhang, X.; Chen, S.; Sun, X.; Zhang, Q.; Luo, Y.; Xie, Y. Optically Switchable Photocatalysis in Ultrathin Black Phosphorus Nanosheets. *J. Am. Chem. Soc.* **2018**, *140*, 3474–3480. [[CrossRef](#)] [[PubMed](#)]
23. Hu, Z.T.; Liu, J.; Yan, X.; Oh, W.D.; Lim, T.T. Low-temperature synthesis of graphene/Bi₂Fe₄O₉ composite for synergistic adsorption-photocatalytic degradation of hydrophobic pollutant under solar irradiation. *Chem. Eng. J.* **2015**, *262*, 1022–1032. [[CrossRef](#)]
24. Zatloukalová, K.; Obalová, L.; Koči, K.; Čapek, L.; Matěj, Z.; Šnajdhaufová, H.; Ryczkowski, J.; Słowik, G. Photocatalytic degradation of endocrine disruptor compounds in water over immobilized TiO₂ photocatalysts. *Iran. J. Chem. Chem. Eng. (IJCCCE)* **2017**, *36*, 29–38.

25. Mboula, V.M.; Héquet, V.; Andrès, Y.; Gru, Y.; Colin, R.; Doña-Rodríguez, J.; Pastrana-Martínez, L.; Silva, A.; Leleu, M.; Tindall, A.; et al. Photocatalytic degradation of estradiol under simulated solar light and assessment of estrogenic activity. *Appl. Catal. B Environ.* **2015**, *162*, 437–444. [[CrossRef](#)]
26. Yang, Y.; Luo, L.; Xiao, M.; Li, H.; Pan, X.; Jiang, F. One-step hydrothermal synthesis of surface fluorinated TiO₂/reduced graphene oxide nanocomposites for photocatalytic degradation of estrogens. *Mater. Sci. Semicond. Process.* **2015**, *40*, 183–193. [[CrossRef](#)]
27. Padilha, J.E.; Fazzio, A.; Da Silva, A.J.R. van der Waals Heterostructure of Phosphorene and Graphene: Tuning the Schottky Barrier and Doping by Electrostatic Gating. *Phys. Rev. Lett.* **2015**, *114*, 066803. [[CrossRef](#)]
28. Hu, W.; Wang, T.; Yang, J. Tunable Schottky contacts in hybrid graphene–phosphorene nanocomposites. *J. Mater. Chem. C* **2015**, *3*, 4756–4761. [[CrossRef](#)]
29. Guo, H.; Lu, N.; Dai, J.; Wu, X.; Zeng, X. Phosphorene nanoribbons, phosphorus nanotubes, and van der Waals multilayers. *Journal of Physical Chemistry C* **2014**, *118*, 14051–14059. [[CrossRef](#)]
30. Luo, Y.; Zhang, S.; Chen, W.; Jia, Y. Interlayer coupling effects on electronic properties of the phosphorene/h-BN van der Waals heterostructure: A first principles investigation. *Phys. B Condens. Matter* **2018**, *534*, 51–55. [[CrossRef](#)]
31. Lee, H.U.; Lee, S.C.; Won, J.; Son, B.-C.; Choi, S.; Kim, Y.; Park, S.Y.; Kim, H.-S.; Lee, Y.-C.; Lee, J. Stable semiconductor black phosphorus (BP)/titanium dioxide (TiO₂) hybrid photocatalysts. *Sci. Rep.* **2015**, *5*, srep08691. [[CrossRef](#)]
32. Liu, H.; Neal, A.T.; Zhu, Z.; Luo, Z.; Xu, X.; Tomanek, D.; Ye, P.D. Phosphorene: An Unexplored 2D Semiconductor with a High Hole Mobility. *ACS Nano* **2014**, *8*, 4033–4041. [[CrossRef](#)] [[PubMed](#)]
33. Wang, H.; Yang, X.; Shao, W.; Chen, S.; Xie, J.; Zhang, X.; Wang, J.; Xie, Y. Ultrathin Black Phosphorus Nanosheets for Efficient Singlet Oxygen Generation. *J. Am. Chem. Soc.* **2015**, *137*, 11376–11382. [[CrossRef](#)] [[PubMed](#)]
34. León, A.; Reuquen, P.; Garín, C.; Segura, R.; Vargas, P.; Zapata, P.; Orihuela, P.A. FTIR and Raman Characterization of TiO₂ Nanoparticles Coated with Polyethylene Glycol as Carrier for 2-Methoxyestradiol. *Appl. Sci.* **2017**, *7*, 49. [[CrossRef](#)]
35. Nawaz, M.; Miran, W.; Jang, J.; Lee, D.S. One-step hydrothermal synthesis of porous 3D reduced graphene oxide/TiO₂ aerogel for carbamazepine photodegradation in aqueous solution. *Appl. Catal. B Environ.* **2017**, *203*, 85–95. [[CrossRef](#)]
36. Woomer, A.H.; Farnsworth, T.W.; Hu, J.; Wells, R.A.; Donley, C.L.; Warren, S.C. Phosphorene: Synthesis, Scale-Up, and Quantitative Optical Spectroscopy. *ACS Nano* **2015**, *9*, 8869–8884. [[CrossRef](#)]
37. Ulhaq, Z.S.; Kishida, M. Brain Aromatase Modulates Serotonergic Neuron by Regulating Serotonin Levels in Zebrafish Embryos and Larvae. *Front. Endocrinol.* **2018**, *9*, 230. [[CrossRef](#)]
38. Lee, D.H.; Jo, Y.J.; Eom, H.J.; Yum, S.; Rhee, J.S. Nonylphenol induces mortality and reduces hatching rate through increase of oxidative stress and dysfunction of antioxidant defense system in marine medaka embryo. *Mol. Cell. Toxicol.* **2018**, *14*, 437–444. [[CrossRef](#)]
39. Ren, X.; Lu, F.; Cui, Y.; Wang, X.; Bai, C.; Chen, J.; Huang, C.; Yang, D. Protective effects of genistein and estradiol on PAHs-induced developmental toxicity in zebrafish embryos. *Hum. Exp. Toxicol.* **2012**, *31*, 1161–1169. [[CrossRef](#)]
40. Alvarez-Corena, J.R.; Bergendahl, J.A.; Hart, F.L. Advanced oxidation of five contaminants in water by UV/TiO₂: Reaction kinetics and by-products identification. *J. Environ. Manag.* **2016**, *181*, 544–551. [[CrossRef](#)]
41. Li, L.; Long, Y.; Chen, Y.; Wang, S.; Wang, L.; Zhang, S.; Jiang, F. Facile synthesis of Fe/Bi₂SiO₅ nanocomposite with enhanced photocatalytic activity for degradation of 17β-Estradiol(E2). *Solid State Sci.* **2018**, *83*, 143–151. [[CrossRef](#)]
42. Fernández, L. Impact of operating conditions on the removal of endocrine disrupting chemicals by membrane photocatalytic reactor. *Environ. Technol.* **2014**, *35*, 2068–2074. [[CrossRef](#)] [[PubMed](#)]
43. Vijayabalan, A.; Selvam, K.; Velmurugan, R.; Swaminathan, M. Photocatalytic activity of surface fluorinated TiO₂-P25 in the degradation of Reactive Orange 4. *J. Hazard. Mater.* **2009**, *172*, 914–921. [[CrossRef](#)] [[PubMed](#)]

Disclaimer/Publisher’s Note: The statements, opinions and data contained in all publications are solely those of the individual author(s) and contributor(s) and not of MDPI and/or the editor(s). MDPI and/or the editor(s) disclaim responsibility for any injury to people or property resulting from any ideas, methods, instructions or products referred to in the content.